Journal of Zhejiang University-SCIENCE B (Biomedicine & Biotechnology) in press
www.jzus.zju.edu.cn; www.springer.com/journal/11585
E-mail: jzus_b@zju.edu.cn

Research Article

https://doi.org/10.1631/jzus.B2500788

Structural basis of calcium-sensing receptor activation by extracellular modulators

Xueli ZENG[1,2*], Hongnan LIU[1*], Xizhe WANG[1*], Zhihong LIU[1,2✉], Yang GAO[1✉]

[1] *Department of Cardiology of Sir Run Run Shaw Hospital and Liangzhu Laboratory, Zhejiang University School of Medicine, Hangzhou 310016, China*
[2] *National Clinical Research Center of Kidney Diseases, Jinling Hospital, Affiliated Hospital of Medical School, Nanjing University, Nanjing 210002, China*

Abstract: The calcium-sensing receptor (CaSR) plays a central role in maintaining systemic calcium homeostasis. In the treatment of secondary hyperparathyroidism (SHPT) associated with chronic kidney disease (CKD), CaSR is targeted by calcimimetic drugs. Recent cryo-electron microscopy (cryo-EM) studies have begun to reveal how CaSR is modulated by various allosteric modulators and signals through G proteins. However, the mechanisms of CaSR activation by the novel calcimimetic, upacicalcet, and the aminoglycoside antibiotic, neomycin, remain elusive. In this study, we present high-resolution cryo-EM structures of human CaSR homodimer complexed with either upacicalcet or neomycin. Coupled with functional studies, it is revealed that both drugs target the extracellular region of the receptor. Upacicalcet occupies the amino-acid binding site of the Venus Flytrap (VFT) domain promoting VFT closure, whereas neomycin occupies a calcium-binding site at the homodimer interface at the base of the VFT, thus inducing the proximity of the two protomers. These findings reveal distinct molecular mechanisms of CaSR modulation by drug molecules, highlight the diversity of ligand-dependent regulatory modes, and provide a structural foundation for the rational design of future CaSR-targeting therapeutics.

Key words: Calcium-sensing receptor (CaSR); Upacicalcet; Neomycin; Cryo-electron microscopy (Cryo-EM)

1 Introduction

The calcium-sensing receptor (CaSR), a class C G protein-coupled receptor (GPCR), is a master regulator of systemic calcium ion (Ca^{2+}) homeostasis (Hofer and Brown, 2003). By sensing extracellular Ca^{2+} concentration fluctuations, CaSR modulates parathyroid hormone (PTH) secretion and renal calcium reabsorption and excretion, while it also participates in diverse physiological processes including gastrointestinal nutrient sensing, bone metabolism, insulin secretion, and neuronal development (Cianferotti et al., 2015; Owen et al., 2016; Riccardi and Brown, 2010; Ruat and Traiffort, 2013; Squires et al., 2014). The dysregulation of CaSR function has significant pathological consequences (Actkins et al., 2021; Grant et al., 2012). Gain-of-function mutations cause autosomal dominant hypocalcemia (ADH1), characterized by hypocalcemia and hypoparathyroidism, whereas loss-of-function mutations lead to familial hypocalciuric hypercalcemia (FHH) or neonatal severe

✉ Yang GAO, gaoyang7@zju.edu.cn
Zhihong LIU, liuzhihong@zju.edu.cn
* These authors contributed equally to this work
Yang GAO, https://orcid.org/0000-0002-8758-0954
Zhihong LIU, https://orcid.org/0000-0001-6093-0726
Xueli ZENG, https://orcid.org/0009-0005-3859-2253
Hongnan LIU, https://orcid.org/0000-0003-1397-4202
Xizhe WANG, https://orcid.org/0009-0008-3042-6666

Received Nov. 30, 2025; Revision accepted Jan. 24, 2026;
Crosschecked xxx. xx, 20xx; Published online xxx. xx, 20xx

hyperparathyroidism (NSHPT) (Chang et al., 2020; Hannan et al., 2018, 2012).

CaSR functions as an obligate homodimer, with each protomer comprising an extracellular domain (ECD) and a heptahelical transmembrane (7TM) domain (TMD) (Gorvin, 2023). The ECD consists of a Venus flytrap (VFT) module and a cysteine-rich domain (CRD). The VFT binds ligands including Ca^{2+}, amino acids and polyamines, transmitting signals through CRD to the TMD, resulting in G protein coupling (Tian et al., 2024). Recent cryo-electron microscopy (cryo-EM) studies have revealed that activation by Ca^{2+} and L-tryptophan (L-Trp) induces VFT closure, resulting in the 7TM homodimer rearranging from an extended parallel conformation to a tightly packed asymmetric configuration (Chen et al., 2021; Gao et al., 2021; Ling et al., 2021; Wen et al., 2021). 7TM positive allosteric modulators (PAMs) such as cinacalcet and evocalcet stabilize this asymmetry, whereas negative allosteric modulators (NAMs) lock the 7TMs in a symmetric inactive state (Gao et al., 2021). However, aside from 7TM allosteric modulators, CaSR is also targeted at the ECD by the next-generation calcimimetic, upacicalcet, and the aminoglycoside antibiotic, neomycin (Goto et al., 2023; Ward et al., 2002), whose mechanisms of action have remained elusive.

Upacicalcet is a next-generation CaSR PAM that has been clinically approved in Japan in 2021 and completed worldwide phase III clinical trials for the treatment of SHPT in 2025 (Pathalys Pharma, 2025a, 2025b). Recent studies demonstrated that upacicalcet dose-dependently reduces serum intact PTH and calcium levels, with no severe hypocalcemia even at 100-fold effective doses (Goto et al., 2023). Crucially, unlike cinacalcet that inhibits gastrointestinal motility by 50%, upacicalcet exhibits superior gastrointestinal safety (Hamano et al., 2025; Shigematsu et al., 2023). These properties position upacicalcet as a promising therapy for secondary hyperparathyroidism, particularly in patients intolerant to conventional treatments. The aminoglycoside antibiotic neomycin is a known CaSR agonist that is widely used to probe receptor physiology (Ward et al., 2002). Functional studies using native CaSR-expressing parathyroid tissue or heterologous expression systems have shown that CaSR can be stimulated by neomycin (McLarnon et al., 2002), however the underlying mechanism has not been elucidated.

In this study, we present cryo-EM structures of the CaSR homodimer complexed with either upacicalcet or neomycin at nominal global resolutions of 2.45 Å and 2.32 Å, respectively. These structures, coupled with functional studies, illustrate how upacicalcet and neomycin distinctly target and modulate CaSR. Specifically, upacicalcet binds to the amino-acid binding site located at the cleft of the bi-lobed VFT domains, stabilizing an active closed-closed VFT conformation. In contrast, neomycin binds to a negatively charged pocket situated at the cross-protomer VFT-CRD interface where a Ca^{2+} ion would bind and directly induces proximity between the ECDs of the two protomers, thus activating the receptor. These findings reveal distinct modes of CaSR allosteric modulation at the ECD, informing the rational design and optimization of future therapeutics targeting the receptor.

2 Materials and methods

2.1 Construct generation

For recombinant protein expression in baculovirus-infected HEK293F cells, a human CaSR construct (UniProt: P41180, residues 20-894) was codon-optimized and cloned into a modified pEZT vector (Morales-Perez et al., 2016), which contains an N-terminal hemagglutinin (HA) signal peptide followed by a FLAG tag and a 3×Ala linker. For functional assays in mammalian cells, the full-length human CaSR construct was subcloned into pcDNA3.1(+) (Durocher et al., 2001) vector, with the native signal peptide replaced by an N-terminal HA signal peptide followed by a FLAG tag and a 3×Ala linker (Gerace and Moazed, 2015). Mutations were introduced by site-directed mutagenesis.

Bioluminescence resonance energy transfer (BRET)-based assays were performed to quantify the activation of CaSR by allosteric ligands. Specifically, a set of TRUPATH Gα/Gβ/Gγ biosensors (Cat. No. 1000000163, Addgene, Watertown, MA, USA) (Olsen et al., 2020) was used to detect the dissociation of Re-

nilla luciferase-labelled Gαi3 (Gα-RLuc8) and green fluorescent protein-labelled Gγ (Gγ-GFP2) subunits. To maximize the dynamic range of BRET signals, we used the reported optimal Gβ3/Gγ9-GFP2 acceptor with the Gαi3-RLuc8 donor.

2.2 Cell culture and expression

Wild-type (WT) CaSR was expressed by infecting HEK293F cells at a density of 2.2-2.5 × 10^6 cells/mL grown in suspension at 37℃ in the presence of 8% CO_2 in Trans CD01 medium (Cat. No. YYCD01.001, Youyi Biotech, Shanghai, China) with 2% (v/v) culture volume of P2 baculoviruses (Chen et al., 2021; Wen et al., 2021). The Bac-to-Bac baculovirus expression system was employed to generate recombinant baculoviruses encoding CaSR in Sf9 insect cells. At 12 h after infection, the HEK293F cells were supplemented with 10 mM sodium butyrate (Cat. No. 102905018, Sigma-Aldrich, St. Louis, MO, USA) to improve the protein production yield and then incubated at 30℃ for 60 h (Chen et al., 2021; Shen et al., 2021). The cells were collected by centrifugation, then the pellets were snap-frozen in liquid nitrogen and stored at −80℃ until further use.

For functional assays in mammalian cells, HEK293F suspension cells were cultured at 37℃ in the presence of 8% CO_2 in Trans CD01 medium. HEK293F cells were transfected at a density of 1.0 × 10^6 cells/mL using 1,200 ng total DNA at a 1:1:1:1 ratio of receptor : Gα-RLuc8 : Gβ : Gγ-GFP, with a DNA : polyethylenimine (PEI) (Cat. No. 919012, Sigma-Aldrich, St. Louis, MO, USA) ratio of 1: 4 (He et al., 2024a). After 48 h, the cells were collected for functional assays. All the cell lines used in this study were obtained from Shanghai Youyi Biological Technology Co., Ltd. (Shanghai, China).

2.3 Purification of CaSR

For the purification of the upacicalcet-bound CaSR, the cell pellets were thawed in buffer containing 50 mM Tris-HCl (pH 7.5), 150 mM NaCl, 10 mM $CaCl_2$, 15% glycerol, protease inhibitor cocktail (Cat. No. B14003, Bimake Biotechnology Co., Ltd., Shanghai, China), and 10 μM upacicalcet (Cat. No. 124894, MedKoo Biosciences, Inc., Morrisville, NC, USA), and lysed by a Dounce homogenizer. The cell lysate was solubilized with 1% n-dodecyl-β-maltoside (DDM) (Cat. No. D-8823, Biosynth, Staad, Switzerland) and 0.2% cholesteryl hemisuccinate (CHS) (Cat. No. CH210, Anatrace, Maumee, OH, USA) for 2 h at 4℃, followed by centrifugation at 30,000 × g for 40 min. The resulting supernatant was incubated with anti-DYKDDDDK affinity beads (Cat. No. SA042025, Changzhou Tiandirenhe Biotech, Changzhou, China) for 1.5 h at 4℃. The resin was then washed with buffer containing 50 mM Tris-HCl (pH 7.5), 150 mM NaCl, 10 mM $CaCl_2$, 15% glycerol, protease inhibitor cocktail, 10 μM upacicalcet, 0.1% DDM, and 0.02% CHS, and transferred to a gravity-flow column. During the washing process, DDM was gradually replaced with glyco-diosgenin (GDN) (Cat. No. GDN101, Anatrace, Maumee, OH, USA), and the protein was eluted from the column using 3xFLAG elution buffer (Cat. No. SLR01002, Changzhou Tiandirenhe Biotech, Changzhou, China). The eluted protein was concentrated and injected onto a Superose 6 Increase 10/300 GL (Cat. No. 29091596, Cytiva, Marlborough, MA, USA) equilibrated in buffer containing 25 mM HEPES (pH 7.5), 150 mM NaCl, 10 mM $CaCl_2$, 10 μM upacicalcet, and 0.005% GDN. Peak fractions were collected and concentrated for the cryo-EM study.

For the purification of neomycin-bound CaSR, the procedures were identical to those described above, with the sole modification being that 10 μM upacicalcet was replaced by 5 mM neomycin (Cat. No. HY-B0407, MedChemExpress, Monmouth Junction, NJ, USA) and 1 mM L-Trp throughout all steps.

2.4 Cryo-EM data collection and processing

Three microliters of the purified upacicalcet-bound CaSR or neomycin-bound CaSR (upa-bound: 6.1 mg/mL, neo-bound: 15 mg/mL) were applied onto the glow-discharged holey gold grids (UltrAuFoil R1.2/1.3, Au300, Quantifoil Micro Tools GmbH, Jena, Germany). The grids were blotted for 6 s with a blot force of 10 at 4℃, 100% humidity, and then plunge-frozen in liquid ethane using Vitrobot Mark IV (Thermo Fisher Scientific, Waltham, MA, USA). Cryo-EM data collection was performed on Titan Krios TEM (Thermo Fisher Scientific, Waltham, MA, USA) at 300 kV accelerating voltage at the Core Facilities, Liangzhu laboratory, Zhejiang

University, equipped with CFEG and Selectris X energy filter, and a Falcon 4 direct electron detector. EPU software was used for automated data collection according to standard procedures. A magnification of 130,000 × was set for imaging, yielding a pixel size of 0.93 Å on images. The defocus range was set from -0.7 to -1.5 μm. Micrographs were recorded for about 2.5 s, with a total exposure dose of approximately 50 electrons per $Å^2$. A total of 5,046 and 15,932 movies were collected for the upacicalcet-bound CaSR and neomycin-bound CaSR, respectively.

All cryo-EM data processing was performed in CryoSPARC v4.6.2 (Punjani et al., 2017). For the upacicalcet-bound CaSR dataset, 1,164,477 particles were picked from 4,369 curated movies originating from 5,046 raw movies. After a round of heterogeneous refinement that yielded 426,841 particles, a final set of 302,092 particles was obtained. Non-uniform refinement of these particles resulted in a consensus map at an overall resolution of 2.45 Å, with subsequent ECD-local and TMD-local refinement improving the resolution of those regions to 2.31 Å and 3.38 Å, respectively. For the neomycin-bound CaSR dataset, 7,378,886 particles were initially picked from 15,181 movies using the same templates with the upacicalcet dataset. A series of heterogeneous refinement rounds narrowed this down to 2,050,902 particles and ultimately to a final stack of 1,432,777 particles. Non-uniform refinement of this final set yielded a consensus map at 2.32 Å, while local refinement produced an ECD-focused map at 2.23 Å and a TMD-focused map at 3.15 Å.

2.5 Model building and refinement

For model building and refinement, the active-state CaSR structures in detergents (PDB ID: 7M3F) were used as the initial models for docking into the cryo-EM maps in Chimera (Pettersen et al., 2004). The models were then subjected to iterative rounds of manual adjustment in Coot v.0.9.8.96 (Emsley et al., 2010) and real-space refinement in PHENIX v.2.0-5847 (Liebschner et al., 2019). The model statistics were validated in MolProbity (Chen et al., 2010). The models of upacicalcet and neomycin were manually built in Coot v.0.9.8.96 and the geometry was further optimized in the eLBOW module of Phenix using the semi-empirical quantum chemical method AM1 option (Moriarty et al., 2009). The restraints generated by eLBOW were implemented in subsequent iterative real-space refinement and validation in Phenix v.2.0-5847. The refinement statistics are provided in Table S1. Chimera and ChimeraX (Pettersen et al., 2021) were used for structure visualization and figure preparation.

2.6 BRET assay using TRUPATH biosensors

The BRET assay for the measurement of G protein activation was performed as previously described, with specific modifications. After 48 hours, cells were collected by centrifugation and washed to remove the cell medium with the assay buffer (Hank's balanced salt solution with 25 mM HEPES pH 7.5). The cells were then resuspended in assay buffer and dispensed into white 96-well plates at a volume of 40 μL per well, followed by the addition of 20 μL coelenterazine 400a (Cat. No. T78389, TargetMol Chemicals Inc, Boston, MA, USA) to achieve a final concentration of 10 μg/mL. Cells were incubated at room temperature for 5 min. Thirty microlitres of ligand solutions, prepared in assay buffer supplemented with 0.1% bovine serum albumin (BSA) (Cat. No. A8020, Solarbio, Beijing, China), were immediately added to plated cells. The detection of upacicalcet required the ligand solution to be supplemented with 1.5 mM Ca^{2+}, a step not required for the detection of neomycin. The plates were read immediately using a Spark Multimode Microplate Reader (Tecan Group Ltd., Männedorf, Switzerland) using 410-nm (RLuc8-coelenterazine 400a) and 515-nm (GFP2) emission filters with a 1-s integration time per well. The BRET ratios were calculated as the ratio of the GFP2 emission to RLuc8 emission. All data were normalized by subtracting the BRET signal recorded at 0 mM Ca^{2+}. Finally, the reaction curve was constructed and generated in GraphPad Prism 10 (GraphPad Software, San Diego, CA, USA). The experiments were performed independently in triplicates.

2.7 Enzyme-linked immunosorbent assay (ELISA)

The cell-surface expression of FLAG-CaSR WT and mutant constructs were evaluated by ELISA (Chen et

al., 2025; Xu et al., 2023; Yamaguchi et al., 2025). After 48 hours post-transfection, HEK293F cells were dispensed into poly-D-lysine-coated 96-well plates at 95 μL per well. Cells were washed with PBS via centrifugation at 500 × g for 3 min, then fixed with 80 μL of 4% paraformaldehyde for 10 min. Following fixation, blocking was performed with 1% (w/v) BSA/PBS for 1 h at room temperature. Afterwards, cells were incubated with a 1:10,000 dilution of anti-FLAG M2 HRP-conjugated monoclonal antibody (Cat. No. AE024, ABclonal Technology, Wuhan, China) in the blocking buffer for an additional 0.5 h at room temperature. Afterwards, the wells were washed three times with blocking buffer and then six times with PBS. Antibody binding was detected using 80 μL/well of the diluent of Super Signal ELISA Femto Maximum Sensitivity Substrate (Cat. No. 37075, Thermo Fisher Scientific, Waltham, MA, USA). The plate was then measured for luminescence using a Spark Cyto microplate reader (Tecan Group Ltd., Männedorf, Switzerland). Finally, the data were normalized to 100% of the WT CaSR using GraphPad Prism 10. The experiments were performed independently in triplicates.

2.8 Statistics and reproducibility

Statistical analyses were performed on data derived from at least three independent experiments using GraphPad Prism 10. For TRUPATH assays, the maximum signal response of the WT group was designated as 100%. Data were normalized as a percentage of this maximal WT response. The half-maximal effective concentration (EC_{50}) was defined as the concentration of ligand eliciting 50% of the maximal response, and pEC_{50} was calculated as $-\log_{10}(EC_{50})$. For ELISA, the protein expression level of the WT group was defined as 100%, and the expression levels of the mutants were normalized relative to WT. Data were presented as mean ± SEM from at least three independent experiments, each performed in triplicate. Statistical significance compared to WT was determined by one-way ANOVA followed by Dunnett's multiple comparisons test (*$P < 0.05$, ** $P < 0.01$, *** $P < 0.001$, **** $P < 0.0001$; ns, not significant ($P > 0.05$). No samples were excluded from the analysis.

3 Results

3.1 Structural determination of CaSR-upacicalcet and CaSR-neomycin complexes

Near full-length human CaSR in HEK293F cells were expressed and the active-state receptor was purified through FLAG-tag affinity and size-exclusion chromatography (Fig. S1). The CaSR-upacicalcet sample was prepared in the presence of 10 μM upacicalcet and 10 mM Ca^{2+}, whereas the CaSR-neomycin sample was purified with 5 mM neomycin, 1 mM L-Trp and 10 mM Ca^{2+}. Cryo-EM analyses of these preparations yielded consensus reconstructions at nominal global resolutions of 2.45 Å for the CaSR-upacicalcet complex and 2.32 Å for the CaSR-neomycin complex (Fig. S2). To further enhance local features, focused refinements were performed on the ECD and TMD of each dataset. The resulting composite maps reached 2.31 Å (ECD) and 3.38 Å (TMD) for the CaSR-upacicalcet complex, and 2.23 Å (ECD) and 3.15 Å (TMD) for the CaSR-neomycin complex. (Fig. S2, Table S1). These high-resolution electron density maps enabled unambiguous atomic model building, detailed analysis of the receptor conformations, and in-depth investigation of the ligand-receptor interactions (Fig. 1 and S3). The cryo-EM map of the CaSR-upacicalcet complex reveals a distinct density of upacicalcet at the amino-acid binding site within the VFT of each protomer, suggesting an activation mechanism reminiscent of that of aromatic amino acids (Fig. 1a and S3a). The cryo-EM map of the CaSR-neomycin complex reveals a prominent non-protein density at the VFT-CRD interface, occupying a Ca^{2+}-binding pocket that has been shown to be critical for CaSR activation. When neomycin was fitted into this density, a terminal sugar ring was not well resolved (Fig. 1b, S3b and S3e), likely due to the inherent conformational flexibility of branched aminoglycosides (Asensio et al., 2002).

3.2 CaSR-upacicalcet complex

Upacicalcet is an amino acid-derived compound featuring an aromatic ring distinct from linear glutathione analogs (Goralski and Ram, 2022), exhibiting structural homology with aromatic amino acids like L-Trp (Goto et al., 2023) (Fig. 2b). Our CaSR-upacicalcet complex structure reveals that upacicalcet binds at the interface between Lobe 1 and Lobe 2 of the VFT, stabilizing the closed ECD conformation (Fig. 1a and 2a). Upacicalcet occupies the same site as L-Trp (Geng et al, eLife) and the recently reported CaSR PAM γ-glutamyl-valyl-glycine (γ-EVG) (Fig. S4) (Yamaguchi et al., 2025). Upacicalcet and γ-EVG utilize the same set of residues to bind to the receptor and their larger sizes compared to L-Trp allow for more extensive interactions (Fig. S4). In the CaSR-upacicalcet complex, residues S170, N64 and R66 from Lobe 1 form polar interactions with the terminal amine (distance, 2.8 Å), the aryl chloride (distance, 3.5 Å), and the sulfonic group (distance, 2.7 Å) of upacicalcet, respectively. Meanwhile, the indole ring of W70 from Lobe 1 forms π-π interaction with the phenyl ring of upacicalcet (distance, 5.1 Å) (Fig. 2b). Accordingly, the S170A, N64A, and W70A mutations all completely abolish the ability of upacicalcet to activate the receptor and the R66A mutation significantly reduces the potency of upacicalcet dose-dependent response (Fig. 2c, 2d and S5a). In Lobe 2, P274 is involved in σ-π interaction with the phenyl group of upacicalcet (distance, 3.8 Å) and E297 forms a salt bridge with the terminal amine (distance, 3.0 Å) (Fig. 2b). Removing the Cβ of P274 by mutating it to a glycine residue causes a right shift of the dose-dependent response curve, whereas the E297A mutation significantly inhibits the activation of CaSR by upacicalcet (Fig. 2c, 2d and S5a). Our structural information along with mutagenesis data reveal that upacicalcet facilitates CaSR activation by tethering the two VFT lobes together through extensive interactions with residues from either side, thus stabilizing the active closed-closed ECD conformation.

3.3 CaSR-neomycin complex

Our CaSR-neomycin complex structure reveals that neomycin, a polycationic aminoglycoside antibiotic, engages CaSR at the interface between VFT and CRD, displacing a Ca^{2+} that has been shown to be critical for CaSR activation (Geng et al., 2016b; Zhang et al., 2016) (Fig. 1b, 3a and S3b). Neomycin is composed of four sugar rings joint linearly by glycosidic bonds (Fig. 3b). Our cryo-EM density resolves the last three sugar rings, whereas the first ring appears to be flexible (Fig. S3e). Neomycin engages the receptor in a V-shaped configuration with the central Ring III, inserting deep into the VFT dimer interface, while the peripheral Rings II and IV bridge the interactions between VFT and CRD from opposite protomers. These interactions primarily involve four acidic residues, namely VFT residues E232 (distance, 2.6 Å) and D234 (distance, 2.5 Å) from one protomer, and VFT residue D238 (distance, 3.8 Å) and CRD residue E588 (distance, 3.1 Å) from the other protomer, each forming polar contacts with neomycin (Fig. 3b). Charge reversal mutations of each of these residues, namely E232K, D234K, D238K and E588K, hamper the activation of CaSR by neomycin to varying degrees, whereas mutating all four residues to lysine (4K) drastically abolish the neomycin response at the receptor (Fig. 3c, 3d and S5b). These functional results are consistent with the modeled neomycin position at the VFT-CRD interface, thus supporting our neomycin placement. Our structure and mutagenesis studies indicate that neomycin activates CaSR by mimicking the function of the Ca^{2+} and engages at a modulation site at the VFT-CRD interface. Neomycin, being a polycationic molecule, binds at this highly acidic site through extensive electrostatic interactions (Fig. S3c), clamping the VFT and CRD from opposing protomers together and stabilizing the compact active ECD configuration.

4 Discussion

CaSR, as the master regulator of human calcium homeostasis, is further involved in nutrient sensing, cardiovascular tone, and insulin secretion (Liu et al., 2018; Schepelmann et al., 2016; Squires et al., 2000). Extensive efforts to target CaSR therapeutically in the past several decades have resulted in clinically approved 7TM PAMs, such as cinacalcet and evocalcet (Nemeth et al., 2018) (Fig. 4). Although these 7TM PAMs can

effectively lower serum PTH and calcium levels, their application is limited by significant gastrointestinal toxicity and the risk of hypocalcemia (Diao et al., 2021). Accordingly, their clinical indications are restricted to SHPT associated with end-stage CKD (Tsai et al., 2024) and hypercalcemia associated with parathyroid carcinoma (Chattopadhyay, 2006). A more recently approved peptide-based PAM, etelcalcetide, binds to the ECD and exhibits an extended half-life suitable for weekly administration; however, it also suffers from similar risks of hypocalcemia compared to cinacalcet (Hamano et al., 2017; Patel and Bridgeman, 2018) (Fig. 4). In the past few years, cryo-EM studies on near full-length human CaSR have illustrated certain molecular mechanisms involving receptor activation by widely used 7TM PAMs (Chen et al., 2021; Gao et al., 2021; Ling et al., 2021; Wen et al., 2021), revealing that the same drug molecule adopts distinct conformations, namely bent and extended, when bound to the two 7TM protomers within the homodimer (Gao et al., 2021) (Fig. 4). This structural information has enabled a recent large-library docking campaign that led to several promising lead compounds with much higher potency than cinacalcet without inducing hypocalcemia in mouse models (Liu et al., 2024). Recently, cryo-EM studies of CaSR-G protein complexes have revealed that upon G protein coupling, the two transmembrane 7TM bundles move closer together with a more tightly packed TM6 interface, with the contact area increasing from 206 Å^2 to 683 Å^2 (He, Wu, Gao, et al., 2024b; Zuo, Park, Frangaj, et al., 2024). Interestingly, both our upacicalcet-bound and neomycin-bound complex structures revealed more tightly packed TMDs compared with the CaSR-cinacalcet complex with TM6 contact areas of 233 Å^2 and 267 Å^2, respectively, and when aligning one 7TM bundle, we could observe a clear downward shift of TM6 in the other 7TM, bringing the conformation closer to the G protein-bound configuration (Fig. S6a and S6b). The observed downward shift suggests that activation by ECD ligands upacicalcet and neomycin may favor G protein activation more than stabilization by clinically used 7TM PAMs such as cinacalcet and evocalcet. Our near-atomic level information of upacicalcet bound to active-state CaSR provides a solid structural platform for future virtual screening efforts. In the meantime, the regulatory site revealed by our CaSR-Neomycin structure offers a distinct mechanism for receptor activity modulation and can enable the structure-based design of more specific and potent drug molecules with distinct pharmacology (Fig. 4). The structural information coupled with functional data presented in this study expands our knowledge of CaSR modulation mechanisms and sheds light on promising future directions for the development of better CaSR-targeting therapeutics.

Data availability statement

All data generated or analysed during this study are included in the Article and its Supplementary Information. Cryo-EM maps for the following reconstructions have been deposited in the Electron Microscopy Data Bank: CaSR-upacicalcet consensus, CaSR-upacicalcet ECD (locally focused-refined), CaSR-upacicalcet TMD (locally focused-refined), CaSR-upacicalcet composite, CaSR-neomycin consensus, CaSR-neomycin ECD (locally focused-refined), CaSR-neomycin TMD (locally focused-refined), and CaSR-neomycin composite, under accession codes EMD-67238, EMD-67236, EMD-67237, EMD-67239, EMD-67243, EMD-67241, EMD-67242, and EMD-67244, respectively. The atomic coordinates of the CaSR-upacicalcet and CaSR-neomycin complexes have been deposited in the Protein Data Bank under accession codes 9XTM and 9XTP, respectively.

Acknowledgments

This work was supported by the National Natural Science Foundation of China (NSFC) under Grant No. 32271240 to Yang GAO, and the Zhejiang Provincial Natural Science Foundation of China under Grant No. LDQ23C05003 to Yang GAO. We thank the staff of the Liangzhu Cryo-EM Facility for their support with data collection.

Author contributions

Xueli ZENG: Investigation, Formal analysis. Hongnan LIU: Writing – original draft, Formal analysis, Data curation, Visualization. Xizhe WANG: Investigation, Visualization. Zhihong LIU: Supervision, Resources, Project administration, Funding acquisition. Yang GAO: Conceptualization, Supervision, Resources, Project administration, Funding acquisition, Writing – revision, Methodology.

Compliance with ethics guidelines

Xueli ZENG，Hongnan LIU，Xizhe WANG，Zhihong LIU and Yang GAO declare that they have no conflicts of interest. This article does not contain any studies with human or animal subjects performed by any of the authors.

Declaration on the use of generative AI tools

No generative AI tools were used in the preparation of this manuscript.

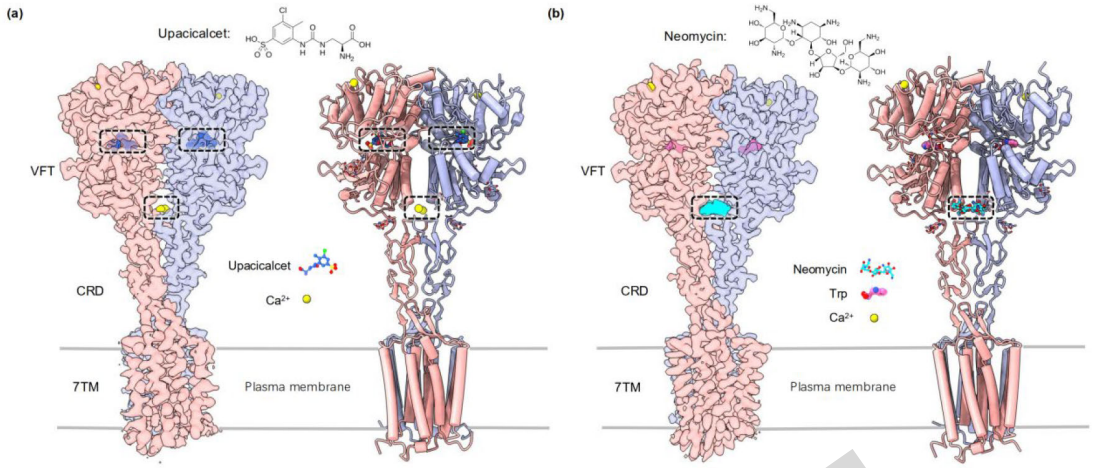

Fig. 1 Cryo-EM structures of the active-state calcium-sensing receptor (CaSR) complexes. Cryo-EM maps (left) and corresponding models (right) of CaSR bound to upacicalcet (a) and neomycin (b). The two protomers are colored blue and pink, respectively, and the dashed boxes denote the binding sites of upacicalcet, neomycin and Ca^{2+}. VFT: Venus Flytrap domain; CRD: cysteine-rich domain; 7TM: heptahelical transmembrane domain; Trp: tryptophan.

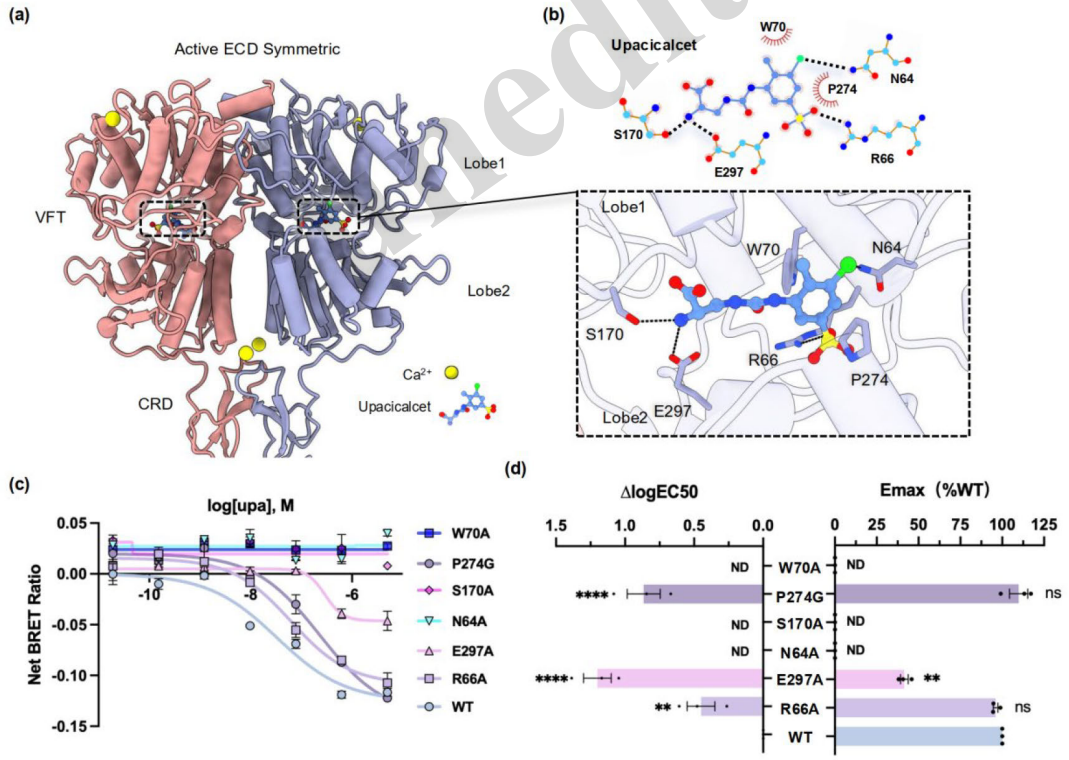

Fig. 2 Upacicalcet binds the Lobe 1-Lobe 2 cleft within each calcium-sensing receptor (CaSR) protomer. (a) Structural model of the CaSR extracellular domain (ECD) in complex with upacicalcet. (b) Close-up view of the upacicalcet-binding pocket in a CaSR protomer, where residues involved in upacicalcet recognition are shown as sticks. (c) Bioluminescence resonance energy transfer (BRET) assays showing that residues distributed across Lobe 1 and Lobe 2 are required for the PAM activity of upacicalcet. (d) Quantification and statistics for panel (c). The bars represent differences in Emax or potency (pEC_{50}) for each mutant, expressed as

a percentage of the wild type (WT) maximum. Data are expressed as mean ±SEM from at least three independent experiments, each performed in technical triplicate. Statistical significance was assessed by one-way ANOVA with Dunnett's multiple comparisons test versus WT (*P< 0.05, ** P < 0.01, *** P < 0.001, **** P < 0.0001; ns, not significant (P > 0.05)). ND, not determined. VFT: Venus Flytrap domain; CRD: cysteine-rich domain.

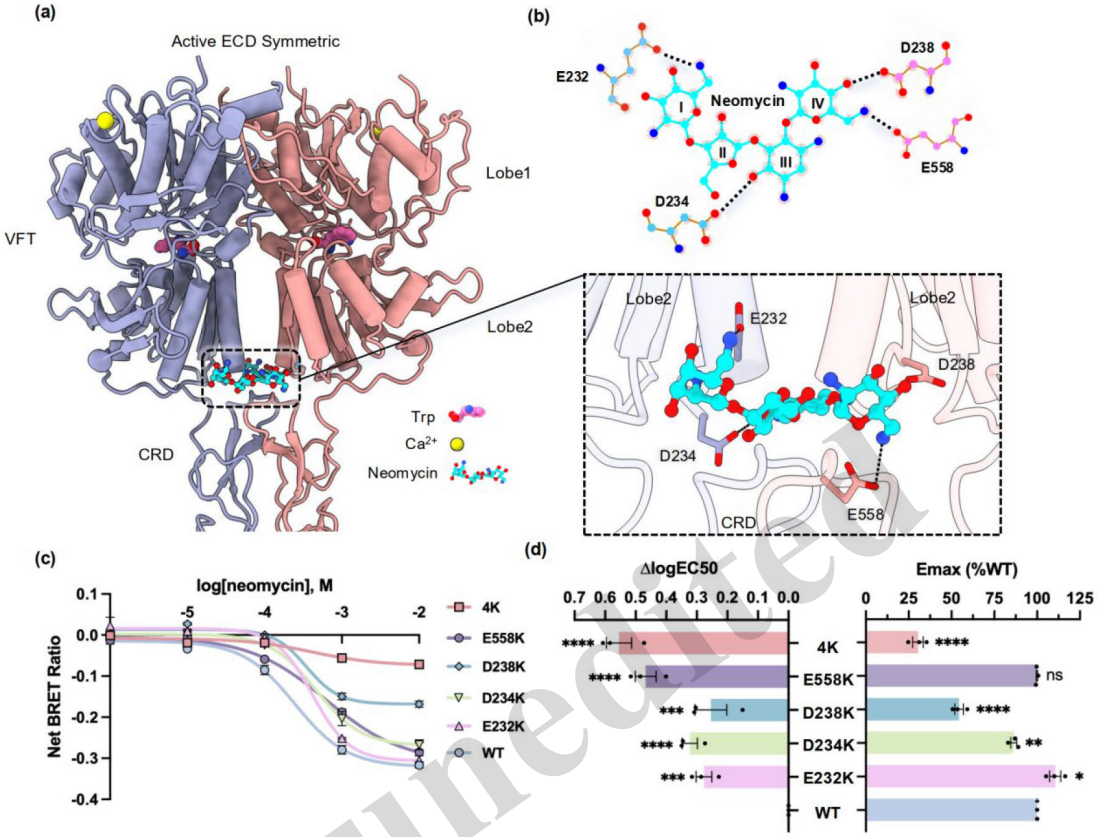

Fig. 3 Neomycin binds to negatively charged clefts at the Lobe 2 interface of the calcium-sensing receptor (CaSR) dimer. (a) Structural model of the CaSR extracellular domain (ECD) in complex with neomycin. (b) Close-up view of the neomycin-binding pocket at the Lobe 2 interface; residues involved in neomycin recognition are shown as sticks. (c) Bioluminescence resonance energy transfer (BRET) assays demonstrating that negatively charged residues within the neomycin-binding pocket are critical for its agonist activity. (d) Quantification and statistics for panel (c). Bars represent differences in E_max or potency (pEC_{50}) for each mutant, expressed as a percentage of the WT maximum. Data are mean ± SEM from at least three independent experiments, each performed in technical triplicate. Statistical significance was assessed by one-way ANOVA with Dunnett's multiple comparisons test versus WT (*P < 0.05, ** P < 0.01, *** P < 0.001, **** P < 0.0001; ns, not significant (P > 0.05)). 4K indicates a quadruple mutation in which E558, D238, D234, and E232 were all substituted with lysine (K). VFT: Venus Flytrap domain; CRD: cysteine-rich domain.

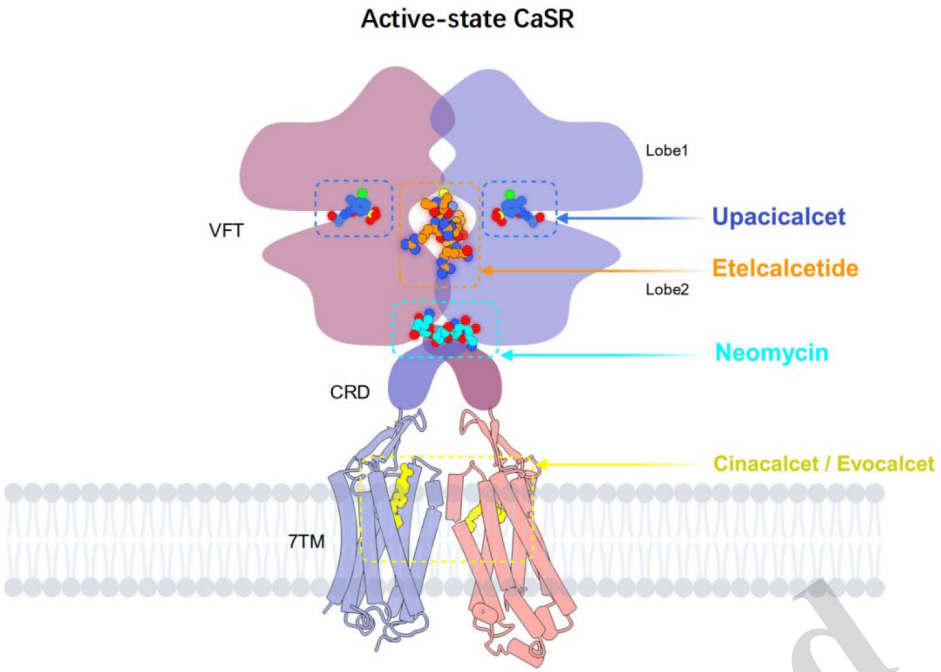

Fig. 4 Schematic overview of ligand-binding sites on the active-state calcium-sensing receptor (CaSR) homodimer—cartoon depiction of an active CaSR dimer embedded in a membrane (grey). The two protomers are colored light blue and light pink. The dashed boxes indicate representative binding loci for clinically used and experimental CaSR ligands: upacicalcet engages the conserved amino acid-binding pocket between Lobe 1 and Lobe 2 of the Venus Flytrap domain (VFT) in each protomer, while neomycin occupies a site at the negatively charged cleft formed at the Lobe-2 interface between protomers. Evocalcet and cinacalcet bind within the heptahelical transmembrane domain (7TM) allosteric cavity of the transmembrane domain, and etelcalcetide acts at the extracellular region near the dimer interface of the VFT. Ligands are shown as space-filling models for illustration. CRD: cysteine-rich domain. Created with BioRender.com.

References

Actkins, K.V., Beasley, H.K., Faucon, A.B., et al., 2021. Calcium-Sensing Receptor Polymorphisms at rs1801725 Are Associated with Increased Risk of Secondary Malignancies. J Pers Med 11, 642. https://doi.org/10.3390/jpm11070642

Asensio, J.L., Hidalgo, A., Cuesta, I., et al., 2002. Experimental evidence for the existence of non-exo-anomeric conformations in branched oligosaccharides: NMR analysis of the structure and dynamics of aminoglycosides of the neomycin family. Chemistry 8, 5228–5240. https://doi.org/10.1002/1521-3765

Chang, W., Tu, C.-L., Jean-Alphonse, F.G., et al., 2020. PTH hypersecretion triggered by a GABAB1 and Ca^{2+}-sensing receptor heterocomplex in hyperparathyroidism. Nat Metab 2, 243–255. https://doi.org/10.1038/s42255-020-0175-z

Chattopadhyay, N., 2006. Effects of calcium-sensing receptor on the secretion of parathyroid hormone-related peptide and its impact on humoral hypercalcemia of malignancy. American Journal of Physiology-Endocrinology and Metabolism 290, E761–E770. https://doi.org/10.1152/ajpendo.00350.2005

Chen, L.-N., Zhou, H., Xi, K., et al., 2025. Proton perception and activation of a proton-sensing GPCR. Molecular Cell 85, 1640-1657.e8. https://doi.org/10.1016/j.molcel.2025.02.030

Chen, V.B., Arendall, W.B., Headd, J.J., et al., 2010. MolProbity: all-atom structure validation for macromolecular crystallography. Acta Crystallogr D Biol Crystallogr 66, 12–21. https://doi.org/10.1107/S0907444909042073

Chen, X., Wang, L., Cui, Q., et al., 2021. Structural insights into the activation of human calcium-sensing receptor. Elife 10, e68578. https://doi.org/10.7554/eLife.68578

Cianferotti, L., Gomes, A.R., Fabbri, S., et al., 2015. The calcium-sensing receptor in bone metabolism: from bench to bedside and back. Osteoporos Int 26, 2055–2071. https://doi.org/10.1007/s00198-015-3203-1

Diao, J., DeBono, A., Josephs, T.M., et al., 2021. Therapeutic Opportunities of Targeting Allosteric Binding Sites on the Calcium-Sensing Receptor. ACS Pharmacol. Transl. Sci. 4, 666–679. https://doi.org/10.1021/acsptsci.1c00046

Durocher, Y., Perret, S., Kamen, A., 2001. Recombinant Protein Production by Transient Transfection of Suspension-Growing Cells, in: Merten, O.-W., Mattanovich, D., Lang, C., Larsson, G., Neubauer, P., Porro, D., Postma, P., de Mattos, J.T., Cole,

J.A. (Eds.), Recombinant Protein Production with Prokaryotic and Eukaryotic Cells. A Comparative View on Host Physiology: Selected Articles from the Meeting of the EFB Section on Microbial Physiology, Semmering, Austria, 5th–8th October 2000. Springer Netherlands, Dordrecht, pp. 331–337. https://doi.org/10.1007/978-94-015-9749-4_24

Emsley, P., Lohkamp, B., Scott, W.G., et al., 2010. Features and development of Coot. Acta Crystallogr D Biol Crystallogr 66, 486–501. https://doi.org/10.1107/S0907444910007493

Gao, Y., Robertson, M.J., Rahman, S.N., et al., 2021. Asymmetric activation of the calcium-sensing receptor homodimer. Nature 595, 455–459. https://doi.org/10.1038/s41586-021-03691-0

Geng, Y., Mosyak, L., Kurinov, I., et al., 2016. Structural mechanism of ligand activation in human calcium-sensing receptor. Elife 5, e13662. https://doi.org/10.7554/eLife.13662

Gerace, E., Moazed, D., 2015. Affinity Pull-Down of Proteins Using Anti-FLAG M2 Agarose Beads. Methods Enzymol 559, 99–110. https://doi.org/10.1016/bs.mie.2014.11.010

Goralski, T., Ram, J.L., 2022. Extracellular Calcium Receptor as a Target for Glutathione and Its Derivatives. Int J Mol Sci 23, 717. https://doi.org/10.3390/ijms23020717

Gorvin, C.M., 2023. Recent advances in calcium-sensing receptor structures and signaling pathways. Prog Mol Biol Transl Sci 195, 121–135. https://doi.org/10.1016/bs.pmbts.2022.06.014

Goto, M., Nishimura, G., Sato, H., et al., 2023. Pharmacological profile of upacicalcet, a novel positive allosteric modulator of calcium-sensing receptor, in vitro and in vivo. Eur J Pharmacol 956, 175936. https://doi.org/10.1016/j.ejphar.2023.175936

Grant, M.P., Stepanchick, A., Breitwieser, G.E., 2012. Calcium signaling regulates trafficking of familial hypocalciuric hypercalcemia (FHH) mutants of the calcium sensing receptor. Mol Endocrinol 26, 2081–2091. https://doi.org/10.1210/me.2012-1232

Hamano, N., Komaba, H., Fukagawa, M., 2017. Etelcalcetide for the treatment of secondary hyperparathyroidism. Expert Opin Pharmacother 18, 529–534. https://doi.org/10.1080/14656566.2017.1303482

Hamano, T., Koiwa, F., Isaka, Y., et al., 2025. Long-Term Efficacy and Safety of Upacicalcet in Japanese Hemodialysis Patients with Secondary Hyperparathyroidism: Open-Label 52-Week Study. Am J Nephrol 56, 70–84. https://doi.org/10.1159/000541493

Hannan, F.M., Kallay, E., Chang, W., et al., 2018. The calcium-sensing receptor in physiology and in calcitropic and noncalcitropic diseases. Nat Rev Endocrinol 15, 33–51. https://doi.org/10.1038/s41574-018-0115-0

Hannan, F.M., Nesbit, M.A., Zhang, C., et al., 2012. Identification of 70 calcium-sensing receptor mutations in hyper- and hypo-calcaemic patients: evidence for clustering of extracellular domain mutations at calcium-binding sites. Hum Mol Genet 21, 2768–2778. https://doi.org/10.1093/hmg/dds105

He, F., Wu, C.-G., Gao, Y., et al., 2024. Allosteric modulation and G-protein selectivity of the Ca2+-sensing receptor. Nature 626, 1–8. https://doi.org/10.1038/s41586-024-07055-2

Hofer, A.M., Brown, E.M., 2003. Extracellular calcium sensing and signalling. Nat Rev Mol Cell Biol 4, 530–538. https://doi.org/10.1038/nrm1154

Liebschner, D., Afonine, P.V., Baker, M.L., et al., 2019. Macromolecular structure determination using X-rays, neutrons and electrons: recent developments in Phenix. Acta Crystallogr D Struct Biol 75, 861–877. https://doi.org/10.1107/S2059798319011471

Ling, S., Shi, P., Liu, S., et al., 2021. Structural mechanism of cooperative activation of the human calcium-sensing receptor by Ca^{2+} ions and L-tryptophan. Cell Res 31, 383–394. https://doi.org/10.1038/s41422-021-00474-0

Liu, F., Wu, C.-G., Tu, C.-L., et al., 2024. Large library docking identifies positive allosteric modulators of the calcium-sensing receptor. Science 385, eado1868. https://doi.org/10.1126/science.ado1868

Liu, G., Cao, W., Jia, G., et al., 2018. Calcium-sensing receptor in nutrient sensing: an insight into the modulation of intestinal homoeostasis. Br J Nutr 120, 881–890. https://doi.org/10.1017/S0007114518002088

Liu, Y., Cao, C., Huang, X.-P., et al., 2023. Ligand recognition and allosteric modulation of the human MRGPRX1 receptor. Nat Chem Biol 19, 416–422. https://doi.org/10.1038/s41589-022-01173-6

McLarnon, S., Holden, D., Ward, D., et al., 2002. Aminoglycoside antibiotics induce pH-sensitive activation of the calcium-sensing receptor. Biochem Biophys Res Commun 297, 71–77. https://doi.org/10.1016/s0006-291x(02)02133-2

Morales-Perez, C.L., Noviello, C.M., Hibbs, R.E., 2016. Manipulation of Subunit Stoichiometry in Heteromeric Membrane Proteins. Structure 24, 797–805. https://doi.org/10.1016/j.str.2016.03.004

Moriarty, N.W., Grosse-Kunstleve, R.W., Adams, P.D., 2009. electronic Ligand Builder and Optimization Workbench (eLBOW): a tool for ligand coordinate and restraint generation. Acta Crystallogr D Biol Crystallogr 65, 1074–1080. https://doi.org/10.1107/S0907444909029436

Nemeth, E.F., Van Wagenen, B.C., Balandrin, M.F., 2018. Discovery and Development of Calcimimetic and Calcilytic Compounds. Prog Med Chem 57, 1–86. https://doi.org/10.1016/bs.pmch.2017.12.001

Olsen, R.H.J., DiBerto, J.F., English, J.G., et al., 2020. TRUPATH, an open-source biosensor platform for interrogating the GPCR transducerome. Nat Chem Biol 16, 841–849. https://doi.org/10.1038/s41589-020-0535-8

Owen, J.L., Cheng, S.X., Ge, Y., et al., 2016. The Role of the Calcium-Sensing Receptor in Gastrointestinal Inflammation. Semin Cell Dev Biol 49, 44–51. https://doi.org/10.1016/j.semcdb.2015.10.040

Patel, J., Bridgeman, M.B., 2018. Etelcalcetide (Parsabiv) for Secondary Hyperparathyroidism in Adults With Chronic Kidney Disease on Hemodialysis. P T 43, 396–399.

Pathalys Pharma, 2025a. A Phase 3 Randomized, Double-Blind, Placebo-Controlled Study Evaluating the Efficacy and Safety of Dose-Titrated PLS240 in the Treatment of Secondary Hyperparathyroidism in Individuals With End Stage Kidney Disease on Hemodialysis (PATH-2) With an Open-Label Extension (Clinical trial registration No. NCT05836220). clinicaltrials.gov.

Pathalys Pharma, 2025b. A Phase 3 Randomized, Double-Blind, Placebo-Controlled Study Evaluating the Efficacy and Safety of Dose-Titrated PLS240 in the Treatment of Secondary Hyperparathyroidism in Individuals With End Stage Kidney Disease on Hemodialysis (PATH-1) With an Open-Label Extension (Clinical trial registration No. NCT05832931). clinicaltrials.gov.

Pettersen, E.F., Goddard, T.D., Huang, C.C., et al., 2021. UCSF ChimeraX: Structure visualization for researchers, educators, and developers. Protein Sci 30, 70–82. https://doi.org/10.1002/pro.3943

Pettersen, E.F., Goddard, T.D., Huang, C.C., et al., 2004. UCSF Chimera--a visualization system for exploratory research and analysis. J Comput Chem 25, 1605–1612. https://doi.org/10.1002/jcc.20084

Punjani, A., Rubinstein, J.L., Fleet, D.J., et al., 2017. cryoSPARC: algorithms for rapid unsupervised cryo-EM structure determination. Nat Methods 14, 290–296. https://doi.org/10.1038/nmeth.4169

Riccardi, D., Brown, E.M., 2010. Physiology and pathophysiology of the calcium-sensing receptor in the kidney. Am J Physiol Renal Physiol 298, F485–F499. https://doi.org/10.1152/ajprenal.00608.2009

Ruat, M., Traiffort, E., 2013. Roles of the calcium sensing receptor in the central nervous system. Best Pract Res Clin Endocrinol Metab 27, 429–442. https://doi.org/10.1016/j.beem.2013.03.001

Schepelmann, M., Yarova, P.L., Lopez-Fernandez, I., et al., 2016. The vascular Ca2+-sensing receptor regulates blood vessel tone and blood pressure. Am J Physiol Cell Physiol 310, C193-204. https://doi.org/10.1152/ajpcell.00248.2015

Shen, C., Mao, C., Xu, C., et al., 2021. Structural basis of GABAB receptor–Gi protein coupling. Nature 594, 594–598. https://doi.org/10.1038/s41586-021-03507-1

Shigematsu, T., Koiwa, F., Isaka, Y., et al., 2023. Efficacy and Safety of Upacicalcet in Hemodialysis Patients with Secondary Hyperparathyroidism. Clin J Am Soc Nephrol 18, 1300–1309. https://doi.org/10.2215/CJN.0000000000000253

Squires, P.E., Harris, T.E., Persaud, S.J., et al., 2000. The extracellular calcium-sensing receptor on human beta-cells negatively modulates insulin secretion. Diabetes 49, 409–417. https://doi.org/10.2337/diabetes.49.3.409

Squires, P.E., Jones, P.M., Younis, M.Y.G., et al., 2014. The calcium-sensing receptor and β-cell function. Vitam Horm 95, 249–267. https://doi.org/10.1016/B978-0-12-800174-5.00010-7

Tian, L., Andrews, C., Yan, Q., et al., 2024. Molecular regulation of calcium-sensing receptor (CaSR)-mediated signaling. Chronic Dis Transl Med 10, 167–194. https://doi.org/10.1002/cdt3.123

Tsai, S.-H., Kan, W.-C., Jhen, R.-N., et al., 2024. Secondary hyperparathyroidism in chronic kidney disease: A narrative review focus on therapeutic strategy. Clin Med (Lond) 24, 100238. https://doi.org/10.1016/j.clinme.2024.100238

Ward, D.T., McLarnon, S.J., Riccardi, D., 2002. Aminoglycosides increase intracellular calcium levels and ERK activity in proximal tubular OK cells expressing the extracellular calcium-sensing receptor. J Am Soc Nephrol 13, 1481–1489. https://doi.org/10.1097/01.asn.0000015623.73739.b8

Wen, T., Wang, Z., Chen, X., et al., 2021. Structural basis for activation and allosteric modulation of full-length calcium-sensing receptor. Sci Adv 7, eabg1483. https://doi.org/10.1126/sciadv.abg1483

Xu, P., Huang, S., Krumm, B.E., et al., 2023. Structural genomics of the human dopamine receptor system. Cell Res 33, 604–616. https://doi.org/10.1038/s41422-023-00808-0

Yamaguchi, H., Kitajima, S., Suzuki, H., et al., 2025a. Cryo-EM structure of the calcium-sensing receptor complexed with the kokumi substance γ-glutamyl-valyl-glycine. Sci Rep 15, 3894. https://doi.org/10.1038/s41598-025-87999-1

Zhang, C., Zhang, T., Zou, J., et al., 2016. Structural basis for regulation of human calcium-sensing receptor by magnesium ions and an unexpected tryptophan derivative co-agonist. Sci Adv 2, e1600241. https://doi.org/10.1126/sciadv.1600241

Supplementary information

Figs. S1–S6; Table S1